

Space-time coupled stability of optical solitons in a nonlinear resonator consisting of periodic layered Kerr media

Sheng Zhang^{1†}, Zongyuan Fu^{1†}, Bingbing Zhu^{1†}, Guangyu Fan², Shunjia Wang¹, Yudong Chen¹,
Yaxin Liu¹, Andrius Baltuska², Chuanshan Tian¹, Zhensheng Tao^{1*}

¹*State Key Laboratory of Surface Physics and Department of Physics, Fudan University, Shanghai, China*

²*Institute of Photonics, TU Wien, Gusshausstrasse 27/387, Vienna, Austria*

[†]These authors contributed equally to this work.

*Corresponding authors: Dr. Zhensheng Tao, ZhenshengTao@fudan.edu.cn.

Abstract

The dynamics and stabilization of solitons are essential for a large variety of fundamental processes in nonlinear optics, condensed matter physics and biology. Taking the solitary propagation of femtosecond pulses in periodic layered Kerr media as an example, we investigate the space-time coupling of optical solitons in a nonlinear resonator. A universal relationship between the beam size and the critical nonlinear phase of the solitary modes is revealed, defining different regions of the resonator stability. Space-time coupling is shown to strongly influence the spectral, spatial and temporal profiles of femtosecond pulses. The sustainable propagation of femtosecond pulses with a GW peak power is demonstrated on resonance, which can be regarded as temporally confined spatial solitons. Taking advantages of the unique characters of these solitary modes, we demonstrate single-stage supercontinuum generation and compression of femtosecond pulses from initially 170 fs down to 22 fs with an efficiency >90%. We also provide evidence of efficient mode self-cleaning which suggests rich spatial-temporal self-organization processes of laser beams in a nonlinear resonator.

Solitons are localized light or matter wave packets propagating with a stable structure in a nonlinear medium, thanks to the balance between the linear (dispersion, diffraction, etc.) and nonlinear effects. Fundamentally, understanding the formation of solitons is important, because they represent stable solutions for the cubic nonlinear Schrödinger equations (NLSE) [1,2], which is related to many branches of physics [3,4]. A very significant contribution to the experimental and theoretical studies of solitons has been in nonlinear optics, especially in Kerr media. It is well known that propagation of strong optical pulses in a Kerr medium is necessarily accompanied by self-focusing when the peak power P is greater than the critical power

$$P_{cr} = \frac{\lambda^2}{2\pi n_0 n_2} \quad [5],$$

with n_0 and n_2 the linear and nonlinear components of the refractive index.

As a result, the formation of spatial solitons under Kerr nonlinearity can be achieved by balancing diffraction with self-focusing. Besides the efforts in searching for optical solitons in a homogeneous nonlinear medium [2,6–9], in recent years, techniques with periodic management of nonlinearity have opened new possibilities [10], and seen penetration into many branches of science [11–13].

In particular, propagation of strong femtosecond pulses in periodic layered Kerr media (PLKM) is a prototypical example of such nonlinearity management. Theory has predicted that it is possible to have solitary spatial modes in PLKMs [14–16]. Experimentally, repetitive variation of the beam profiles for $P \approx 6 P_{cr}$ has been observed without spatial beam collapse [17]. Ultimately, such periodic propagation of femtosecond pulses can be considered as two-dimensional transverse [(2+1)D] spatial solitons in a mirrorless nonlinear resonator [15], but the stability of these solitons could be strongly influenced by the space-time coupling of femtosecond pulses. To date, no experimental studies on such spatiotemporal propagation exist.

Understanding the general features of the multidimensional coupling of solitons in PLKM resonators could benefit the studies on solitons under similar periodic “potentials” in many other fields of nonlinear optics, including waveguide arrays [18,19], periodic refractive-index gratings [20,21] and photonic crystal fibers [22], as well as in condensed matter physics [11,12] and in biology [13].

On the other hand, in general practice of nonlinear optics, the propagation of strong laser pulses in a condensed medium is limited by the low MW critical power of materials, although high-energy femtosecond lasers with GW peak power have become attainable nowadays. The self-focusing effect beyond the critical power results in violent growth of pulse intensity, causing catastrophic beam collapse and optical damage. It has been shown that at an appropriate ionization level, defocusing from plasma can cancel self-focusing, resulting in filamentary beam propagation in air [23] and in condensed media [24,25]. Nevertheless, the peak power deliverable in this process is limited to $\sim 10P_{cr}$ before the occurrence of multiple filamentation [26]. Stabilizing the solitary beam propagation in PLKM resonators can also harness the enormous potential to greatly enhance long-range nonlinear light-matter interaction, with a power much higher than the critical power.

In this Letter, we experimentally characterize the space-time coupled propagation of femtosecond pulses with a peak power reaching GW in a nonlinear resonator comprising PLKM. By comparing the experimental and theoretical results, we interrogate the resonator stability conditions. A universal relationship between the characteristic beam size and the critical nonlinear phase of the solitary modes is revealed, under which the propagation of light wave-packets can be regarded as temporally confined spatial solitons. Different regions for the

resonator stability are distinguished, manifested by the correlated variations of femtosecond pulses in the spectral, spatial and temporal profiles. In practice, we demonstrate two applications of these solitary modes – First, taking advantages of the sustainable and high-intensity soliton propagation in PLKMs, we suppress the spatial loss, and achieve supercontinuum generation (SCG) and pulse compression with ~90% efficiency, which is much higher than the recent multiplate SCG studies [27–30]. Second, spatial mode-self-cleaning with high efficiency is demonstrated when the beam propagation is on resonance, which can be attributed to the spatial self-organizing effect in a nonlinear resonator.

The repetitive propagation of a high-intensity laser beam in PLKM can be regarded as a cavity resonator with non-spherical (Kerr-lens) mirrors (see Fig. 1(a)). In order to search for the self-consistent spatial modes on resonance, we first resort to the Fresnel-Kirchhoff diffraction (FKD) integral without considering the space-time coupling. Assuming the normalized amplitude of the incident optical field as U_1 , we derive that the amplitude, after propagating through a unit of the resonator and right before the next period, is given by

$$U_2(\rho) = -2\pi j e^{j\pi\rho^2} \int_0^\infty U_1(\rho') e^{jb|U_1(\rho')|^2} \cdot e^{j\pi\rho'^2} J_0(2\pi\rho'\rho) \rho' d\rho', \quad (1)$$

where ρ and ρ' are the radial coordinates rescaled by $\sqrt{\lambda L}$ and J_0 the zeroth-order Bessel function. Here, one period of the resonator contains a layer of Kerr medium with a thickness of l and the following layer of free space by length L . In Eq. (1), b represents the nonlinear phase given by $b = \frac{2\pi}{\lambda} n_2 I_0$, where I_0 is the field intensity. The Fox-Li iteration is then used to numerically find the resonant modes [31], the nonlinear phase associated with which is defined as the critical nonlinear phase b_c . As shown in Fig. 1(b), the characteristic properties of a nonlinear resonator are determined by the beam radius (w) on the layers, the resonator length

(L) and the critical nonlinear phase (b_c). Here, we define a Fresnel-number-like beam radius squared $w^2/\lambda L$, for convenience of discussion.

For our experimental studies, we employed a Yb:KGW amplifier laser system with a pulse duration of 170 fs at $\lambda=1030$ nm. Transform-limited femtosecond pulses with p polarization are focused to a beam waist of 140 μm (see Supplementary Materials (SM) for the experimental setup). The PLKM is composed of polycrystalline Al_2O_3 thin plates as the Kerr medium, placed at the Brewster angle to minimize the loss on each plate $<0.5\%$. The nominal thickness of the plates is fixed to be 0.4 mm (see SM). The input surface of the PLKM is placed at the beam focus, with the distance between the neighboring plates equal to the resonator length L . By adjusting the incident pulse energy, the resonant modes are experimentally identified. The spatial beam profiles within PLKM is monitored with a 4- f imaging setup, while the temporal intensity profiles are measured with a second-harmonic-generation frequency-resolved optical gating (SHG-FROG) setup [32].

First, we present findings on the key features of the resonator stability. The characteristic curve in Fig. 1(b) defines the resonant modes of the PLKM resonators predicted by our FGD model. In the experiments, we observe a reduction of the far-field beam size and an improvement of the spatial mode quality (see SM), as the incident pulse energy (E_{in}) approaches from low to a critical value under a specific resonator length L (e.g. $L=50.8$ mm in the inset of Fig. 1(b)). When the pulse energy is low and the self-focusing in the media is weak, the beam propagation is dominated by diffraction, leading to a diverging beam size on the successive layers (“*unstable diffractive region*” in Fig. 1(b)). On the contrary, when the incident beam can produce the critical nonlinear phase (b_c) to appropriately balance the diffraction ($E_{\text{in}}=260$ μJ for

$L=50.8$ mm, corresponding to a field intensity of 5.0×10^{12} W/cm²), the laser beam can repetitively propagate through the PLKM with a well-confined beam size. Indeed, with the 4- f imaging measurements, we observe that the beam radius approaches a stable value after the self-adjustment in the first few layers under the resonant condition (Fig. 1(d)), which indicates the formation of spatial solitons [15]. The corresponding value of b_c is determined according to the beam radii and pulse durations measured experimentally (see SM). We summarize the experimental results for the solitary modes under different L s in Fig. 1(b), which exhibits excellent agreement with the FKD model. We note that even though the space-time coupling is not taken into account in the FKD model, it still yields very accurate prediction on the solitary modes and the resonant conditions (Fig. 1(b)). This is because the pulse temporal profiles are mostly unchanged and confined, when the propagation is on resonance (see below). The solitary beam propagation on resonance is also confirmed by our (2+1)D NLSE simulations with the cylindrical symmetry [1], which incorporates the space-time coupling, dispersive, the nonlinear Kerr and Raman effects (see SM).

When the nonlinear phase b is higher than the critical value, the beam propagation is more complicated, and the space-time coupling strongly influences the spectral, spatial and temporal profiles of femtosecond pulses (see Fig. 1(a)). In Fig. 2(a), we plot the axial spectral bandwidth as a function of the nonlinear phase for $L=50.8$ mm, in association with the beam size variation. In addition to the spectral broadening owing to self-phase modulation (SPM) [33], the bandwidth saturates at the same critical phase b_c , which can be well reproduced by the 2D NLSE simulations. The corresponding variations of spectra and intensity profiles are shown in Fig. 2(b) and (c). The saturation of the spectral bandwidth is a direct consequence of the SPM

process on a temporally split pulse (Fig. 2(c)). For a positively chirped split pulse, SPM upshifts (downshifts) the frequencies of the trailing (rising) edge of the first (second) pulse, generating new spectral contributions around the fundamental frequency. This observation is also well captured by the 2D NLSE simulations with an accuracy of the incident pulse energy within 10% of the experimental value (Fig. 2(d) and (e)). This result illustrates the correlation between the bandwidth saturation and temporal pulse splitting, due to space-time coupling. We note that such agreement can be achieved for different resonators, indicating the universality of this observation (see SM).

According to the 1D FKD model, there exists a region for $b > b_c$, in which the beam size does not immediately diverge but oscillates, as it propagates through the PLKM (“*quasi-stable oscillatory region*”, see SM). The upper boundary of this region is $P = 2P_{\text{thr}}$, where P_{thr} is given by $P_{\text{thr}} = P_{\text{cr}} \gamma n_0$ [16]. The geometrical factor γ is given by $\gamma = \frac{L}{l}$. Beyond $2P_{\text{thr}}$, the strong Kerr lens breaks the balance between the self-focusing and diffraction, and the beam size grows out of limit within few periods of propagation (“*unstable dissipative region*”). Experimentally, the oscillatory region is manifested by the energy range above b_c where the beam size stays close to its minimum value. However, the width of this region is generally narrower than the FKD results (see the inset of Fig. 1(b) and SM), which can be attributed to the temporal pulse splitting above resonance (Fig. 2(c) and (e)).

The temporal pulse splitting beyond b_c is a result of the spatial cavity mode selection for different pulse intensities in time. When the peak intensity is increased beyond the critical value, the pulse temporal center mismatches with the cavity resonance and experiences fast divergence due to the strong Kerr lensing, which results in splitting of pulses in time and strong conical

emission (Fig. 1(a)). In Fig. 2(f), we show the pulse temporal profiles after each material layer for the conditions on and above the resonance. It clearly shows that, when $E_{\text{in}} = 260 \mu\text{J}$ (on resonance), the femtosecond pulse can maintain almost the same pulse profile and GW peak power, as it propagates through 15 layers of the PLKM. Given that the transverse beam size also remains the same on resonance (Fig. 1(d)), such beam propagation can thus be regarded as a temporally confined (2+1)D spatial soliton. In stark contrast, above the resonance, significant amount of optical energy at the pulse temporal center is scattered away in the form of ring-shaped conical emission, leading to complex pulse splitting (see Fig. 2(f)). The fact that the femtosecond pulse can maintain a stable intensity profile on resonance indicates that the dispersion-induced pulse broadening is negligible. This may be because of the relatively narrow bandwidth of the Yb laser in our experiments, which is different from the previous results using Ti:Sapphire amplifiers [29,34].

Recently, the progress in high-quality SCG with multiple plates of Kerr media has attracted great attention, because of its applications in ultrashort pulse generation [27,29,30,34,35] and optical parametric amplification [28]. However, in the past configurations of the multiplate SCG, the plate thickness and their positions were empirically determined for the broadest spectrum, which makes such a method difficult to be systematically studied and optimized. Strong conical emission [27,29] and spatial nonlinearity [24] due to the complex space-time coupling are shown to cause >40% energy loss, which significantly limits the intensity achievable in practice.

The generation of GW, temporally confined spatial solitons in this work can significantly improve the multiplate SCG and pulse compression. Here, we summarize three advantages.

First of all, as evidenced in Fig. 1(d) and Fig. 2(f), the solitary mode can maintain the high intensity of femtosecond pulses throughout the propagation in PLKMs, supporting sustainable nonlinear light-matter interaction over many layers of the Kerr media. As an example, we send 260 μJ , 170 fs pulses through a 15-layer PLKM with $L = 50.8$ mm under the resonant condition. The spectrum of the output pulse is significantly broadened, corresponding to a transform-limited (TL) pulse duration of 22 fs. The chirp of the output pulses is then compensated by a set of chirped mirrors which supplies a negative second-order group-delay dispersion of -1200 fs^2 over 850-1200 nm. The duration of the compressed pulses from this single-stage compressor is close to the TL pulse (see Fig. 3(a)). The experimental and reconstructed FROG traces are shown in Fig. 3(b) and (c), respectively. We note that our result represents the greatest number of layers implemented in a single-stage multiplate SCG experiment, and the SCG bandwidth is about 50% broader than the previous work under the similar conditions [30]. Second and more importantly, the spatial loss induced by conical emission is strongly suppressed by the solitary propagation. As shown in Fig. 3(d), the conical radiation only contributes $<10\%$ of the total output energy when the propagation is on resonance, and this contribution can increase to $\sim 35\%$ in the dissipative region (Fig. 3(e)). If we consider the transmission efficiency ($\sim 92\%$ without spatial filtering, and $\sim 85\%$, if we remove the conical emission), the single-stage compressor produces ~ 5 times increment of the peak power (Fig. 3(a)). We note that He *et al.* recently reported high efficiency in their multiplate SCG ($\sim 85\%$), and interestingly, the 7 plates in their work had the same thickness and the laser intensity on many plates was the same [34]. We believe it is possible that the beam propagation was close to the resonant condition in that work, similar to our observation here. At last, the single-peaked temporal profile on resonance (Fig.

2(f)) also avoids high-order dispersion induced by SPM, which circumvents the usage of custom-designed chirped mirrors or the low-efficiency pulse shapers [29,30]. This is evidenced by the fact that the clean pulse compression (Fig. 3(a)) is achieved by only compensating the second-order dispersion.

Finally, we show the spatial mode self-cleaning from the nonlinear PLKM resonator. The improvement of the output spatial mode, in terms of the circularity and the intensity profile, can already be observed after the fundamental laser beam passing through the PLKM (see SM). To further investigate the mode-self-cleaning effect, we introduce substantial perturbation on the beam profile, by inserting a cylindrical beam blocker with a diameter of 0.8mm into the laser beam, which has a full-width-of-half-maximum (FWHM) size of ~ 3 mm (Fig. 4(a)). The spatially modulated laser beam is then focused into a resonator with $b_c=0.5$, $L=25.4$ mm, consisting of 20 layers. As shown in Fig. 4(b-d), by matching with the cavity resonance, the output mode is significantly cleaned and transforms to the resonator solitary mode. In Fig. 4(e), we plot the filtering efficiency as a function of the blocker transverse position Δx , with larger Δx inducing greater spatial modulation (Fig. 4(a)). The PLKM resonator can support a high filtering efficiency ($>85\%$) across a large range of spatial modulation, in direct contrast to an ideal linear spatial filter (see SM). This result suggests that the solitary modes here represents attractors of the (2+1)D cubic NLSE equation [3]. There must be an efficient pathway, in which the laser energy in the higher-order spatial modes can be transferred to the solitary modes through the repetitive Kerr interactions. This is consistent with the spatial self-organization of laser beams, previously observed under the nonlinear interactions in filamentation [36], self-focusing collapse [37] and multimode fibers [38,39].

In summary, we experimentally investigate the spatiotemporal propagation of strong laser beams in PLKM resonators and reveal its influence on the stability of optical solitons. Taking advantages of the unique characters of these solitary modes, we demonstrate high-efficiency SCG, pulse compression and spatial mode-self-cleaning. These results are relevant to a wide range of applications, such as Kerr-lens mode locking [40], ultrashort-pulse generation [27,29,30] and high-energy wavelength scaling [28]. Moreover, the results here illustrate the general features of the space-time coupling of solitons under periodically modulated Kerr nonlinearity, which may reinforce the theory and help understanding soliton formation under the influence of other kinds of nonlinearity, e. g. the 2D solitons stabilized by the Feshbach resonance in a Bose-Einstein condensation [12].

Reference

- [1] C. Sulem and P. L. Sulem, *The Nonlinear Schrödinger Equation* (Springer, 1999).
- [2] R. Y. Chiao, E. Garmire, and C. H. Townes, *Phys. Rev. Lett.* **2**, 479 (1966).
- [3] E. Infeld and G. Rowlands, *Nonlinear Waves, Solitons and Chaos*, 1st ed. (Cambridge University Press, 1990).
- [4] P. A. Robinson, *Rev. Mod. Phys.* **69**, 507 (1997).
- [5] R. W. Boyd, *Nonlinear Optics*, 3rd ed. (Academic Press, Inc., 2008).
- [6] V. Zakharov and A. Rubenchik, *Sov. Phys. JETP* **38**, 494 (1974).
- [7] W. E. Torruellas, Z. Wang, D. J. Hagan, E. W. VanStryland, G. I. Stegeman, L.

- Torner, and C. R. Menyuk, Phys. Rev. Lett. **73**, 1632 (1995).
- [8] M. Soljačić, S. Sears, and M. Segev, Phys. Rev. Lett. **81**, 4851 (1999).
- [9] G. C. Duree, J. L. Shultz, G. J. Salamo, M. Segev, A. Yariv, B. Crosignani, P. Di Porto, E. J. Sharp, and R. R. Neurgaonkar, Phys. Rev. Lett. **71**, 533 (1993).
- [10] B. A. Malomed, *Soliton Management in Periodic Systems* (Springer-Verlag, Berlin, 2006).
- [11] Y. Sivan, G. Fibich, and M. I. Weinstein, Phys. Rev. Lett. **97**, 193902 (2006).
- [12] H. Saito and M. Ueda, Phys. Rev. Lett. **90**, 040403 (2003).
- [13] A. S. Davydov, J. Theor. Biol. **66**, 379 (1977).
- [14] L. Bergé, V. K. Mezentsev, J. J. Rasmussen, P. L. Christiansen, and Y. B. Gaididei, Opt. Lett. **25**, 1037 (2000).
- [15] I. Towers and B. A. Malomed, J. Opt. Soc. Am. B **19**, 537 (2002).
- [16] S. N. Vlasov, V. A. Petrishchev, and V. I. Talanov, Izv. Vys- Shikh Uchebnykh Zaved. Radtoftzika **13**, 908 (1970).
- [17] M. Centurion, M. A. Porter, P. G. Kevrekidis, and D. Psaltis, Phys. Rev. Lett. **97**, 033903 (2006).
- [18] H. S. Eisenberg, Y. Silberberg, R. Morandotti, A. R. Boyd, and J. S. Aitchison, Phys. Rev. Lett. **81**, 3383 (1998).
- [19] D. N. Christodoulides and R. I. Joseph, Opt. Lett. **13**, 794 (1988).
- [20] J. W. Fleischer, T. Carmon, M. Segev, N. K. Efremidis, and D. N. Christodoulides, Phys. Rev. Lett. **90**, 023902 (2003).
- [21] D. Neshev, E. Ostrovskaya, Y. Kivshar, and W. Krolikowski, Opt. Lett. **28**, 710

- (2003).
- [22] D. V. Skryabin, F. Luan, J. C. Knight, and P. S. J. Russell, *Science* **301**, 1705 (2003).
- [23] A. Braun, X. Liu, G. Korn, D. Du, J. Squier, and G. Mourou, *Opt. Lett.* **20**, 73 (1995).
- [24] L. Bergé, S. Skupin, R. Nuter, J. Kasparian, and J. P. Wolf, *Reports Prog. Phys.* **70**, 1633 (2007).
- [25] L. Sudrie, A. Couairon, M. Franco, B. Lamouroux, B. Prade, S. Tzortzakis, and A. Mysyrowicz, *Phys. Rev. Lett.* **89**, 1 (2002).
- [26] A. Couairon and A. Mysyrowicz, *Phys. Rep.* **441**, 47 (2007).
- [27] Y. Cheng, C. Lu, Y. Lin, and A. H. Kung, *Opt. Express* **24**, 7224 (2016).
- [28] N. Ishii, P. Xia, T. Kanai, and J. Itatani, *Opt. Express* **27**, 11447 (2019).
- [29] C.-H. Lu, Y.-J. Tsou, H.-Y. Chen, B.-H. Chen, Y.-C. Cheng, S.-D. Yang, M.-C. Chen, C.-C. Hsu, and A. H. Kung, *Optica* **1**, 400 (2014).
- [30] C.-H. Lu, W.-H. Wu, S.-H. Kuo, J.-Y. Guo, M.-C. Chen, S.-D. Yang, and A. H. Kung, *Opt. Express* **27**, 15638 (2019).
- [31] A. G. Fox and T. Li, *IEEE J. Quantum Electron.* **2**, 774 (1966).
- [32] R. Trebino, K. W. DeLong, D. N. Fittinghoff, J. N. Sweetser, M. A. Krumbügel, B. A. Richman, and D. J. Kane, *Rev. Sci. Instrum.* **68**, 3277 (1997).
- [33] R. R. Alfano, *The Supercontinuum Laser Source*, 2nd ed. (Springer, 2006).
- [34] P. He, Y. Liu, K. Zhao, H. Teng, X. He, P. Huang, H. Huang, S. Zhong, Y. Jiang, S. Fang, X. Hou, and Z. Wei, *Opt. Lett.* **42**, 474 (2017).
- [35] M. Seidel, G. Arisholm, J. Brons, V. Pervak, and O. Pronin, *Opt. Express* **24**, 9412 (2016).

- [36] B. Prade, M. Franco, A. Mysyrowicz, A. Couairon, H. Buersing, B. Eberle, M. Krenz, D. Seiffer, and O. Vasseur, *Opt. Lett.* **31**, 2601 (2006).
- [37] K. D. Moll, A. L. Gaeta, and G. Fibich, *Phys. Rev. Lett.* **90**, 203902 (2003).
- [38] K. Krupa, A. Tonello, B. M. Shalaby, M. Fabert, A. Barthélémy, G. Millot, S. Wabnitz, and V. Couderc, *Nat. Photonics* **11**, 237 (2017).
- [39] L. G. Wright, D. N. Christodoulides, and F. W. Wise, *Nat. Photonics* **9**, 306 (2015).
- [40] I. P. Christov, M. M. Murnane, H. C. Kapteyn, and V. D. Stoev, *Opt. Lett.* **20**, 2111 (1995).

Acknowledgement

We thank Aleksei Zheltikov, Huailiang Xu, Andy Kung and Ming-Chang Chen for helpful discussions. The experimental studies were performed at Fudan. We gratefully acknowledge the financial support from the National Natural Science Foundation of China (Grant No. 11874121) and the Shanghai Municipal Science and Technology Basic Research Project (Grant No. 19JC1410900). CS. T. acknowledges support from the National Natural Science Foundation of China (No. 11874123) and the National Key Research and Development Program of China (No. 2016YFA0300902). Z. T. thanks the support from the Alexander-von-Humboldt foundation.

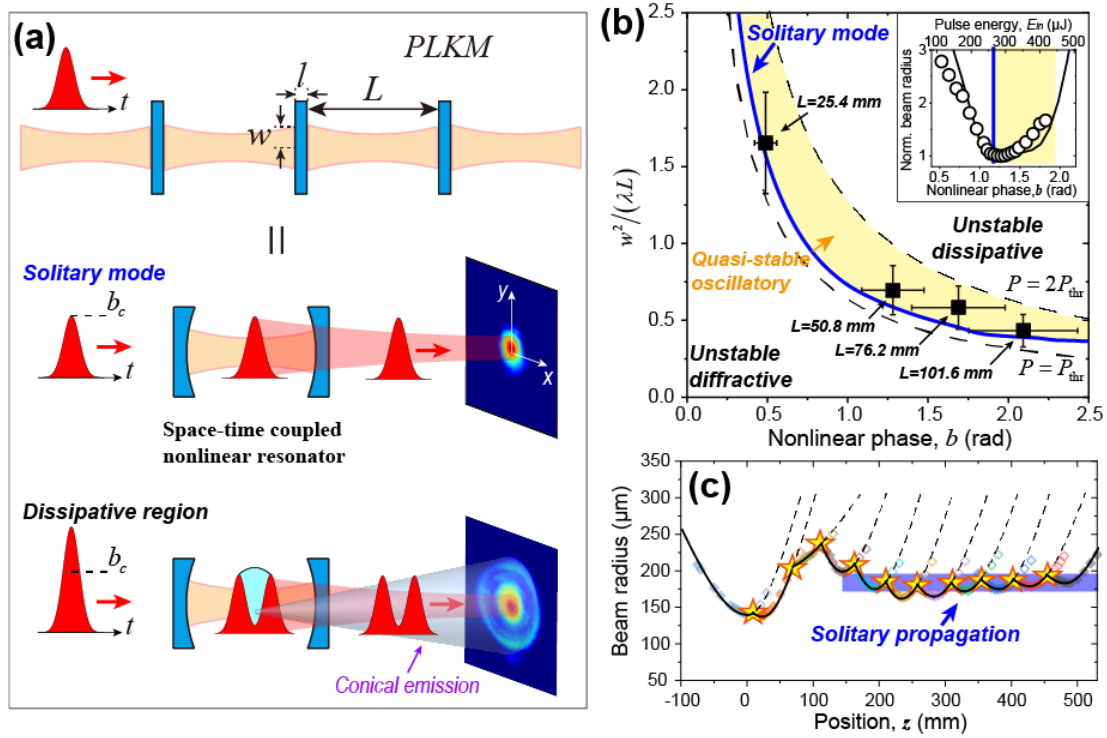


Figure 1. (a) Illustration of the repetitive self-focusing and diverging pattern in PLKM, which is equivalent to a space-time coupled nonlinear optical resonator. The space-time coupled propagation of femtosecond pulses for the solitary modes and in the dissipative region is presented. When the propagation is in the dissipative region, strong conical emission is contributed by the optical energy at the temporal center of the pulse, leading to temporal pulse splitting. (b) Universal relationship of the normalized beam radius squared $w^2/\lambda L$ as a function of the nonlinear phase b for the resonator solitary modes (solid blue line). The dashed lines represent the boundaries for $P_{\text{thr}} < P < 2P_{\text{thr}}$. The symbols are the experimental results with different resonator lengths. The yellow shaded area labels the “quasi-stable oscillatory region”. Inset: Variation of the far-field beam radius as a function of applied nonlinear phase and incident pulse energy for $L=50.8$ mm, $b_c = 1.2$. (c) Experimentally measured beam radii through the propagation in the PLKM with $L=50.8$ mm, $b_c = 1.2$ under the resonant condition. The beam radius on each layer is labeled by the star symbols.

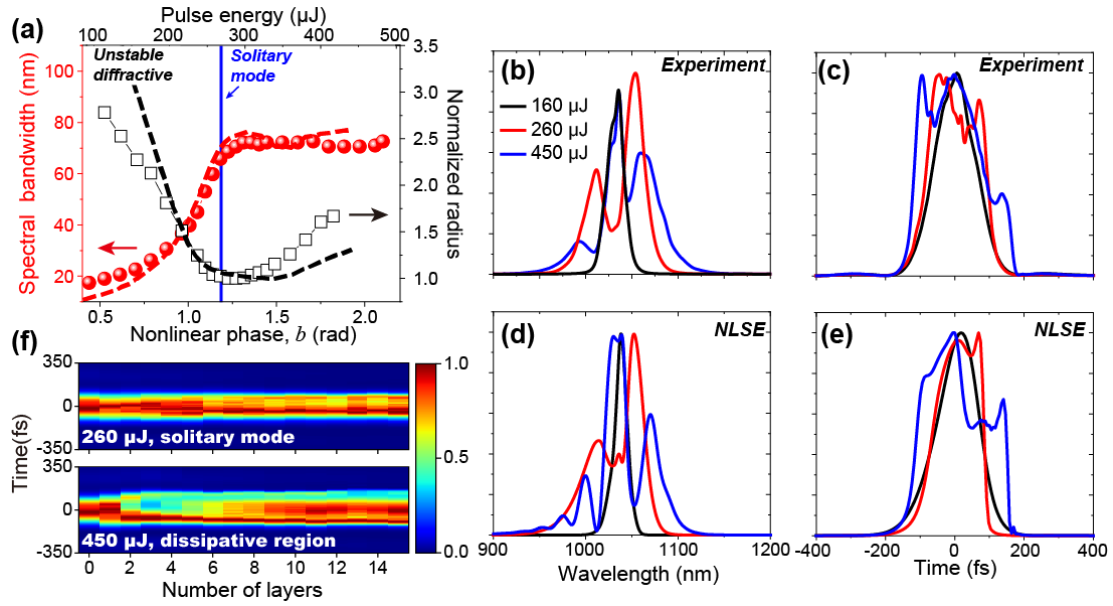


Figure 2. (a) The spectral bandwidth and normalized beam radius as a function of the nonlinear phase and pulse energy for the PLKM resonator with $L=50.8$ mm, 15 layers. The dashed lines are the results of the NLSE simulations. (b-c) The far-field spectral and temporal profiles in different stability regions. (d-e) The NLSE simulation results under the same experimental conditions in (b-c). (f) Evolution of temporal intensity profiles as the pulses propagate through the PLKM on resonance ($E_{\text{in}}=260$ μJ) and above resonance ($E_{\text{in}}=450$ μJ).

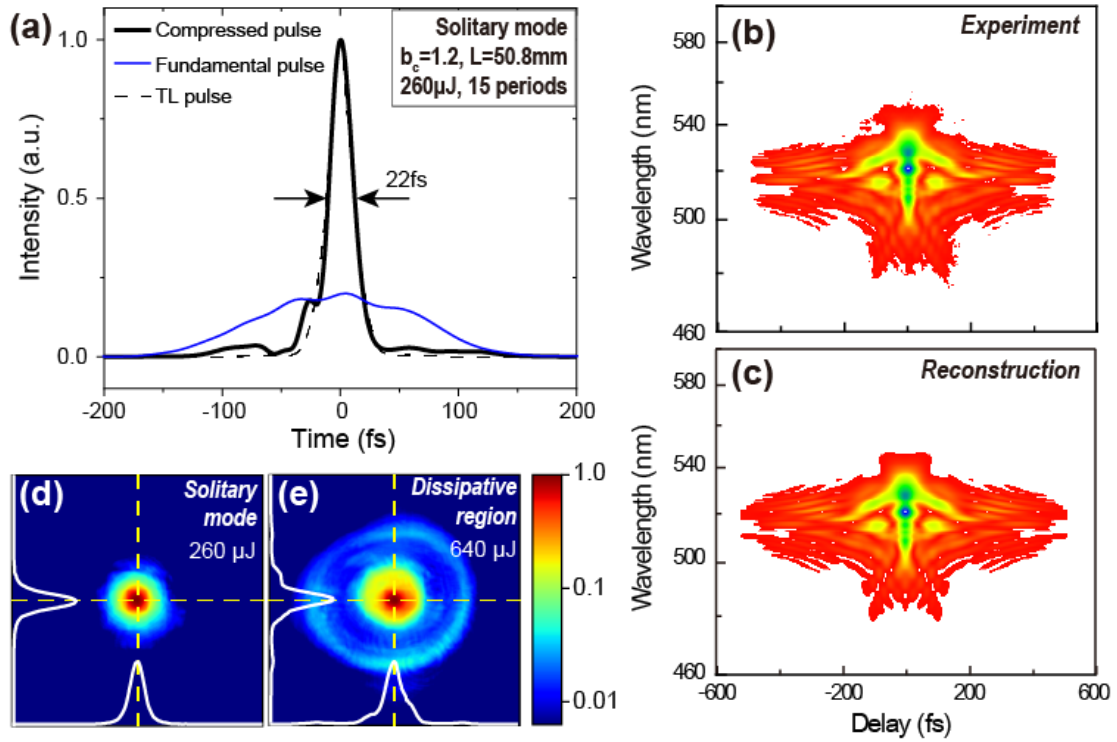


Figure 3. (a) The temporal intensity profiles of the compressed pulse (solid black) and the incident pulse (solid blue). The dashed black line is the TL pulse. (b) and (c) The measured and reconstructed FROG traces. (d) The spatial mode of output beam on resonance ($E_{in} = 260 \mu\text{J}$). The intensity is plotted in log-scale to highlight the conical emission. The white lines display the x and y transverse profiles of the beam. (e) Same as (d) with $E_{in} = 640 \mu\text{J}$ in the dissipative region.

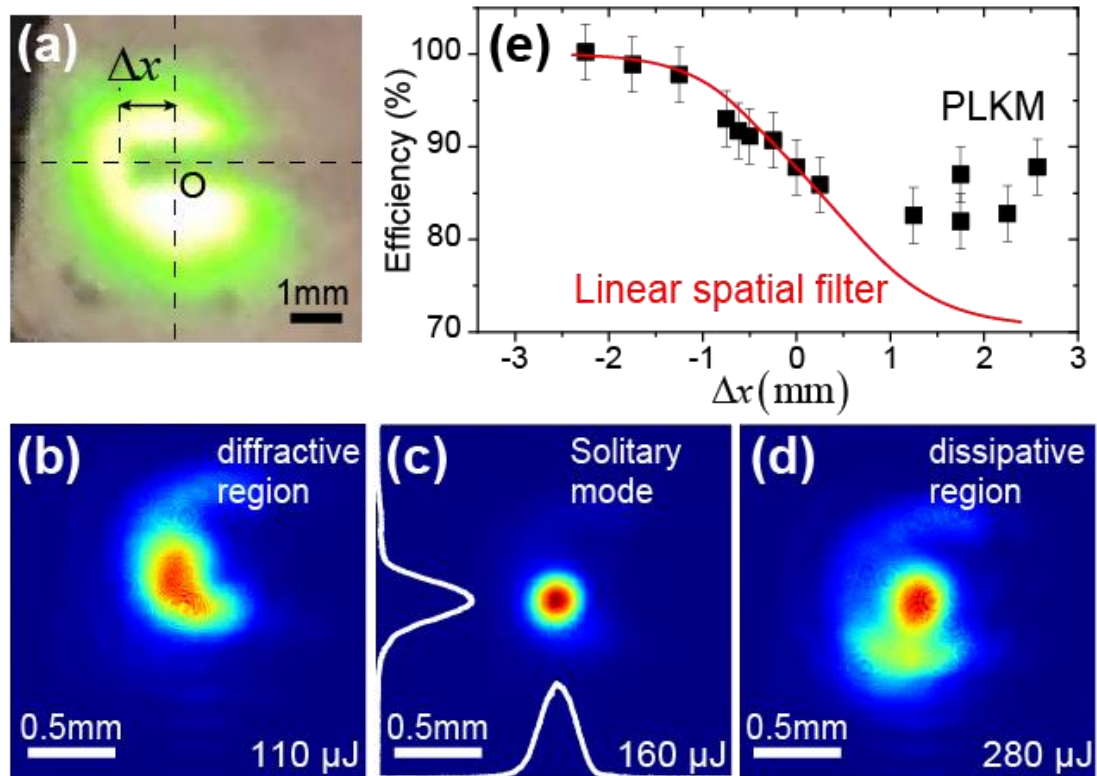


Figure 4. (a) Camera picture of the modulated laser beam after the beam blocker for $\Delta x \approx 1.25$ mm. O is the center of the beam profile and Δx is the transverse blocker position. (b-d) The output beam profiles measured in the far field, for the spatially modulated input beam shown in (a), in the diffractive region, at the solitary mode and in the dissipative region, respectively. The lineouts in (c) represent the horizontal and vertical beam profiles at the solitary mode. (e) The filtering efficiency as a function of the blocker position (Δx) for the PLKM resonator and a linear spatial filter.